Finite-strain elasticity theory and liquid-liquid phase separation in compressible gels

Justin Little,[1] Alex J. Levine,[1,2,3,*] Amit R. Singh,[4] and Robijn Bruinsma[1,2]

[1]*Department of Physics and Astronomy, University of California, Los Angeles, California 90095, USA*
[2]*Department of Chemistry and Biochemistry, University of California, Los Angeles, California 90095, USA*
[3]*Department of Computational Medicine, David Geffen School of Medicine, University of California, Los Angeles, California 90095, USA*
[4]*Department of Mechanical Engineering, Birla Institute of Technology and Science, Pilani, RJ 333031, India*

(Received 21 March 2022; revised 13 October 2022; accepted 21 December 2022; published 27 February 2023)

The theory of finite-strain elasticity is applied to the phenomenon of *cavitation* observed in polymer gels following liquid-liquid phase separation of the solvent, which opens a fascinating window on the role of *finite-strain elasticity theory* in soft materials in general. We show that compressibility effects strongly enhance cavitation in simple materials that obey neo-Hookean elasticity. On the other hand, cavitation phenomena in gels of flexible polymers in a binary solvent that phase separates are surprisingly similar to those of *incompressible* materials. We find that, as a function of the interfacial energy between the two solvent components, there is a sharp transition between cavitation and classical nucleation and growth. Next, biopolymer gels are characterized by *strain hardening* and even very low levels of strain hardening turn out to suppress cavitation in polymer gels that obey Flory-Huggins theory in the absence of strain hardening. Our results indicate that cavitation is, in essence, not possible for polymer networks that show strain hardening.

DOI: 10.1103/PhysRevE.107.024418

I. INTRODUCTION

Biological physics has been enriched by the realization that the physics of phase separation provides insight into segregation phenomena that take place inside cells [1–3]. Examples are the formation of stress granules in the cytoplasm of cells and the formation of nucleoli in the cell nucleus. These membraneless organelles typically contain a high concentration of macromolecules, such as RNA or proteins, that are in a liquid-like state [4–6]. The formation of these structures is triggered by changes in environmental conditions such as concentration, pH, salinity, or temperature.

Cellular separation phenomena have characteristics that set them apart from the well-studied liquid-liquid phase separation of simple binary liquids [7]. A striking example is the absence of *Oswald ripening*, or coarsening, which refers to the growth of larger droplets of the minority phase and a corresponding shrinkage of smaller droplets. It is driven by the interfacial energy between the two components of the liquid [8]. In contrast, liquid-liquid phase separation in cells produces a distribution of droplets with constant radii. This is attributed to the fact that both the cytoplasm of cells and the interior of the cell nucleus are permeated by networks of biopolymers. As confirmed by numerical simulations [9], growth of minority-phase droplets can be stopped by *elastic deformation* of the surrounding polymer network.

The cytoplasm of a cell and the interior of the cell nucleus are both complex environments with complex elastic properties. However, model systems are available in the form of permanently cross-linked synthetic gels with a solvent that is a simple binary liquid [10]. The majority component of the binary liquid is a good solvent for the gel polymers while the minority phase is a poor solvent. Upon phase separation, a relatively monodisperse phase of minority phase droplets appears inside the polymer matrix. For lower levels of supersaturation, droplet growth is indeed arrested by the polymer matrix but the droplets grow in an unlimited fashion when the osmotic pressure of the minority phase exceeds a critical value, which is of the order of the elastic modulus of the polymer network.

An interesting possibility is that this is a form of cavitation, which refers to the swelling of a pressurized cavity inside an elastically deformable material when the pressure exceeds a certain critical value. Cavitation has been observed in rubberlike materials [11] as well as in soft-matter materials [12,13]. Cavitation cannot be understood within the confines of the theory of linear elasticity. It is a consequence of the inherently nonlinear nature of elasticity when the elastic strains no longer are small compared to one. When finite-strain elasticity theory [14] is applied to cavity formation in rubberlike materials, one encounters cavitation with a critical pressure equal to $5/2$ of the shear modulus of the material [11].

In theoretical studies of the cavitation of rubberlike materials, it is assumed that the material is *incompressible*, or nearly so, and this same assumption is also commonly made in theoretical studies of cavitation by liquid-liquid phase separation in polymer gels. The assumption allows for an important simplification: For incompressible materials, the displacement field surrounding a pressurized spherical cavity has a known analytic form that is completely determined by mass conservation. Once this deformation map is known, one

[*]Deceased.

can directly compute the relation between pressure and cavity radius. However, for compressible materials, obtaining the displacement field requires using the mathematical machinery of finite-strain elasticity theory, which leads to an equation for mechanical equilibrium that is of a daunting mathematical complexity.

While the combined system of solvent plus polymers *as a whole* indeed is (nearly) incompressible, osmotic compression and expansion of the polymer matrix with respect to the solvent at fixed total volume certainly is possible. The study of osmotic compression is, in fact, a central feature of the physics of polymer gels [15]. Measured values of the osmotic compressional and shear moduli of gels composed of flexible synthetic polymers typically are comparable to each other [16], so the assumption of incompressibility certainly is not valid—but is compressibility really an important issue for cavitation? Compressibility could drastically alter the deformation and density profiles surrounding the cavity. On the one hand, the density profile could develop a maximum at or near the surface of the swelling cavity due to pile-up of the material that has been pushed out of the cavity (snowplow effect). This could slow down cavitation. On the other hand, as the cavity swells, the density might also develop a minimum at the cavity surface due to the lateral stretching of volume elements (balloon effect) and this could accelerate cavitation. It so happens that in linear elasticity theory, these two effects cancel each other exactly, with the result that in that case the density surrounding a pressurized cavity is uniform. As we shall see, this is certainly not so under the theory of finite-strain elasticity.

An important question about cavitation in biogels involves *strain hardening*. This refers to an increase of the differential shear modulus under increasing levels of shear strain. Strain hardening is not significant for the type of gels on which cavitation experiments have been carried out but it is a known characteristic of biopolymer networks [17]. Strain hardening plays an important role in the biomechanics of cells and tissue. A numerical study of phase separation in a network of biopolymers indicate that strain hardening can suppress cavitation [9]. Synthetic biomimetic hydrogels have been developed with a tunable level of strain hardening [18–21], so it now is possible to study quantitatively the effects of strain hardening.

A final question of interest concerns the relation between cavitation and the classical scenario of droplet nucleation and growth in phase-separating binary liquids. It would seem that when the interfacial energy between the two components of the binary solvent increases, cavitation should somehow transform to the spontaneous growth of droplets with a radius larger than that of the critical nucleus but it is not clear how this transformation takes place.

The aim of this article is to apply finite-strain elasticity theory to explore the effects of compressibility, interfacial energy, and strain hardening on cavitation. In Sec. II we briefly review finite-strain elasticity and discuss the general form of invariant free energy densities. In Sec. III, we apply finite-strain elasticity theory to the simpler case of compressible neo-Hookean materials. There, we also develop a variational method to obtain the deformation map for cavitation in the presence of compressibility, strain hardening and surface tension. The variational method is tested by comparing it with the outcome of a numerical solution of the equations for mechanical equilibrium. In Sec. IV, the variational method is applied to cavitation in gels. We conclude in Sec. V.

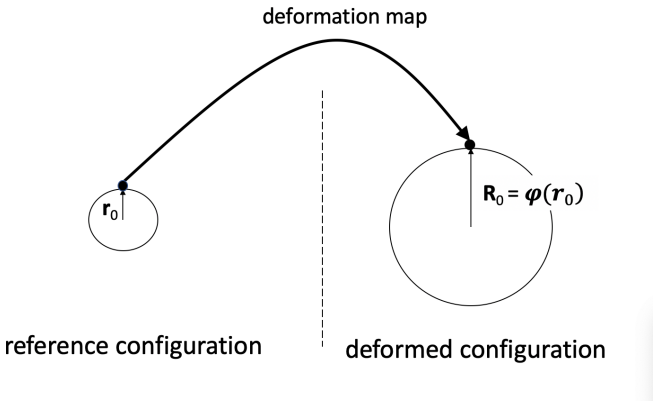

FIG. 1. Schematic deformation map of a spherical cavity that has a radius r_0 in a strain-free reference configuration. When pressurized, the radius of the cavity increases to R_0. The deformation map $\varphi(r)$ relates points in the reference configuration to points in the deformed configuration. The figure shows the mapping for the case of a point on the cavity surface.

II. FINITE-STRAIN ELASTICITY THEORY

Finite-strain elasticity theory can be formulated in different but equivalent ways [14,22,23]. In this section, we review our particular choice.

A. Deformation maps and the Green-Lagrange strain tensor

Consider a material whose internal configuration is defined by the positions of material elements that form a coarse-grained description of the underlying molecular structure of the material. The *reference configuration* $\mathcal{B}_0$ of the material is defined to be a state with neither internal nor external stresses. By assumption, the material elements are uniformly distributed in this state. When the material is exposed to external stress, it deforms into a new configuration $\mathcal{B}$. In the Lagrangian formalism, this deformation is described by a continuous mapping of each position $\vec{x} \in \mathcal{B}_0$ in the reference configuration to a new position $\vec{X} \in \mathcal{B}$ in the deformed configuration:

$$\vec{\varphi} : \vec{x} \mapsto \vec{X}. \tag{1}$$

Figure 1 shows an example of a material that, in the strain-free reference configuration, has a spherical cavity of radius r_0. When this cavity is pressurized it swells up, with a new radius R_0.

The distinction between the reference configuration $\mathcal{B}_0$ and the deformed configuration $\mathcal{B}$ is a key feature of finite-strain elasticity theory: the vectors $\vec{x}$ and $\vec{X}$ live in two distinct vector spaces. In the following, vectors and tensors defined in the reference space will carry Greek indices while vectors and tensors defined in the deformed space will have Latin indices. Final expressions for physical quantities will all be defined on the reference space, i.e., we use a Lagrangian frame of

reference. We also will be using curvilinear coordinate systems for both spaces with $g_{\alpha\beta}$ the metric tensor of the reference space and G_{ij} that of the deformed space. Covariant derivatives in the reference space will be denoted as $\frac{D}{Dx^\alpha}$ while those in the deformed space will be denoted as $\frac{D}{DX^i}$. The associated Christoffel symbols are $\Gamma^\alpha_{\beta\gamma}$, respectively, $\bar{\Gamma}^i_{jk}$.

A line element dx^α in the reference space is transformed into a line element dX^i in the deformed space by the *deformation gradient matrix*:

$$dX^i = A^i{}_\alpha dx^\alpha, \tag{2}$$

with

$$A^i{}_\alpha \equiv \frac{\partial \varphi^i}{\partial x^\alpha}. \tag{3}$$

Note the mixed indices of the deformation gradient matrix. The norm squared of the line element transforms as

$$|d\vec{X}|^2 = A^{i\alpha}A_{i\beta}dx_\alpha dx^\beta \equiv \left(2\mathcal{U}^\alpha_\beta + \delta^\alpha_\beta\right)dx_\alpha dx^\beta. \tag{4}$$

Here

$$\mathcal{U}^\alpha_\beta \equiv \tfrac{1}{2}\left(A^{i\alpha}A_{i\beta} - \delta^\alpha_\beta\right) \tag{5}$$

is the *Green-Lagrange* strain tensor defined on the reference space. Indices are here raised and lowered using the two metric tensors. In the limit of small deformations, the Green-Lagrange strain tensor is conveniently expressed in terms of the *displacement vector*

$$\vec{u}(\vec{x}) = \vec{X} - \vec{x} = \vec{\varphi}(\vec{x}) - \vec{x} \tag{6}$$

of a material point under the action of the force. In the limit $\vec{u} \to 0$, the Green-Lagrange strain tensor reduces to

$$\mathcal{U}^\alpha_{\beta\,\mathrm{lin}} = \tfrac{1}{2}(\partial^\alpha u_\beta + \partial_\beta u^\alpha) + O(u^2), \tag{7}$$

which is the strain tensor of linear elasticity theory [24].

Using the polar decomposition theorem, one can write the deformation gradient A as the product of a rotation matrix R and the symmetric, positive definite matrices U and V:

$$A^i{}_\alpha = R^i{}_\beta U^\alpha_\beta = V^i_j R^j_\alpha. \tag{8}$$

Here, U is defined on the reference space and is referred to as the right stretch tensor, while V, which lives in the deformed space, is the left stretch tensor. The three eigenvalues of U and V are identical and denoted by $\lambda_{i=1,2,3}$. They correspond to the *principal stretch ratios* in the sense that a spherical volume in the reference space is transformed into an ellipsoid in the deformed space whose principal axes are along the directions of the eigenvectors while the stretching ratios along the principal axes are λ_i. Note that $A^{\mathrm{T}}A = U^2$ and $AA^{\mathrm{T}} = V^2$ both have eigenvalues λ_i^2.

A volume element dv in the reference space transforms under the deformation into a volume element dV in the deformed space given by $dV = Jdv$, where J is the Jacobian of the deformation map A. Conservation of mass allows us to write J in terms of the local densities of the material before and after the deformation,

$$\rho dV = \rho_0 dv \Rightarrow J = \frac{\rho_0}{\rho}, \tag{9}$$

so $J = 1$ for incompressible systems. For convenience, the ratio $\rho_r \equiv \frac{\rho}{\rho_0} = \frac{1}{J}$ will be referred to as the relative density. The Jacobian can be expressed as $J = \det A = \det U = \det V = \lambda_1\lambda_2\lambda_3$. In linear elasticity theory, $J \approx 1 + \mathrm{tr}\,\mathcal{U}_{\mathrm{lin}}$. The linear shear strain tensor $\bar{\mathcal{U}}_{\mathrm{lin}}$ is constructed from the linear strain tensor by subtraction of the trace times the unity matrix, so the trace of the shear strain tensor is zero in linear elasticity.

These relations break down for large deformations and the shear strain tensor must be constructed differently. As a first step, consider an area element in the reference space $ds^\alpha = ds\, n^\alpha$, where $\hat{n}$ is the unit vector normal to the area element of the deformation. Under the deformation, a volume element $dx^\alpha ds_\alpha$ transforms as

$$dX^i dS_i = J dx^\alpha ds_\alpha, \tag{10}$$

where $dX^i = A^i{}_\alpha dx^\alpha$. This gives for the transformed area element

$$dS^i = J(A^{-1})^i_\alpha ds^\alpha, \tag{11}$$

where A^{-1} is the inverse deformation gradient matrix:

$$(A^{-1})^\alpha_i \equiv \frac{\partial(\varphi^{-1})^\alpha}{\partial X^i}. \tag{12}$$

Next, write a general deformation mapping $\vec{\varphi}$ as the product of two successive mappings:

$$\vec{\varphi}(\vec{x}) = \vec{\varphi}_{\mathrm{shr}}(\vec{\varphi}_{\mathrm{cmp}}(\vec{x})). \tag{13}$$

The first map $\vec{\varphi}_{\mathrm{cmp}}(\vec{x})$ is here a pure dilation given by

$$\vec{\varphi}_{\mathrm{cmp}}(\vec{x}) = J^{1/3}\vec{x}, \tag{14}$$

with J the Jacobian of the full deformation $\vec{\varphi}$. The second map $\vec{\varphi}_{\mathrm{shr}}$ is a volume-preserving shear. Using the chain rule, the deformation gradient matrix of the full map $\vec{\varphi}$ is

$$A^i{}_\alpha = \frac{\partial \varphi^i_{\mathrm{shr}}}{\partial \varphi^\beta_{\mathrm{cmp}}}\frac{\partial \varphi^\beta_{\mathrm{cmp}}}{\partial x^\alpha} = J^{1/3}\bar{A}^i{}_\alpha. \tag{15}$$

The new deformation gradient matrix $\bar{A}$ is volume preserving since

$$\det \bar{A} = \det(J^{-1/3}A) = \frac{1}{J}\det A = 1. \tag{16}$$

The associated Green-Lagrange shear strain tensor is then

$$\begin{aligned}\bar{\mathcal{U}}^\alpha_\beta &= \tfrac{1}{2}\left(\bar{A}^{i\alpha}\bar{A}_{i\beta} - \delta^\alpha_\beta\right) = \tfrac{1}{2}\left(J^{-2/3}A^{i\alpha}A_{i\beta} - \delta^\alpha_\beta\right)\\ &= J^{-2/3}\mathcal{U}^\alpha_\beta + \tfrac{1}{2}(J^{-2/3} - 1)\delta^\alpha_\beta.\end{aligned} \tag{17}$$

While this nonlinear shear strain tensor is volume preserving, it is—unlike its linearized counterpart—not traceless. The trace of the shear strain tensor will play a central role in the following.

For the cavitation problem, one assumes spherical symmetry. The reference configuration $\mathcal{B}_0$ will be defined as a strain-free state that has a spherical cavity with radius r_0 at the center. The cavity is then pressurized with a pressure P. The new configuration $\mathcal{B}$ is described by a mapping from a material point at $(r, \theta, \phi) \in \mathcal{B}_0$ to the new location $(\varphi(r), \theta, \phi) \in \mathcal{B}$ (see Fig. 1). The radius of the swollen cavity in $\mathcal{B}$ is then $R_0 = \varphi(r_0)$. Recall that the density $\rho(R)$ of the deformed material is related to that of the undeformed material by the Jacobian $J(R) = \frac{\rho_0}{\rho(R)} = 1/\rho_r$. It follows that

$\rho(R)R^2dR = \rho_0 r^2 dr$, which gives $\rho_r = \frac{r^2}{\varphi(r)^2\varphi'(r)}$. For an incompressible system with fixed Jacobian $J = 1$, this reduces to the differential equation $\varphi'(r) = \frac{r^2}{\varphi(r)^2}$ with solution $\varphi(r) = (R_0^3 + r^3 - {r_0}^3)^{1/3}$. For spherical symmetry, the deformation gradient matrix, Jacobian, and strain tensor reduce—in spherical coordinates—to

$$A^i_{\ \alpha} = \frac{\partial \varphi^i}{\partial x^\alpha} = \begin{pmatrix} \varphi' & 0 & 0 \\ 0 & 1 & 0 \\ 0 & 0 & 1 \end{pmatrix}, \tag{18}$$

$$J = \sqrt{\frac{\det G}{\det g}}\det A = \frac{\varphi^2}{r^2}\varphi', \tag{19}$$

$$\mathcal{U}^\alpha_\beta = \frac{1}{2}\begin{pmatrix} \varphi'^2 - 1 & 0 & 0 \\ 0 & \frac{\varphi^2}{r^2} - 1 & 0 \\ 0 & 0 & \frac{\varphi^2}{r^2} - 1 \end{pmatrix}, \tag{20}$$

$$\mathrm{tr}\,\mathcal{U} = \frac{\varphi^2}{r^2} + \frac{1}{2}\varphi'^2 - \frac{3}{2}. \tag{21}$$

Finally, the trace of the shear strain tensor is

$$\mathrm{tr}\,\bar{\mathcal{U}} = J^{-2/3}\left(\frac{\varphi^2}{r^2} + \frac{1}{2}\varphi'^2\right) - \frac{3}{2}. \tag{22}$$

An important part of finite-strain elasticity theory are the definitions of the different stress tensors that can enter in the equation for mechanical equilibrium [see Eq. (A5)]. The variational method that we will use does not involve the stress tensor. For completeness, the different versions of the stress tensor are briefly reviewed in Appendix A.

B. Elastic free-energy densities

In finite-strain elasticity theory, the free-energy density of a material is, in general, expressed as a combination of scalar quantities obtained from the strain tensor $\mathcal{U}$ that are invariant under coordinate transformations. The lowest-order invariant is the trace $\mathrm{tr}\,\mathcal{U}$ of the strain tensor. This invariant can be expressed in terms of the principle stretch ratios λ_i as $\frac{1}{2}(\sum_{i=1}^3 \lambda_i^2 - 3)$ (in the engineering literature, this invariant is normally denoted as I_1). Next, the Jacobian $J = \lambda_1\lambda_2\lambda_3$ is a cubic invariant that enters in the equation of state of materials. Contributions to the free-energy density that only depend on the density ρ_r can be expressed in terms of $J = 1/\rho_r$. Finally, free-energy densities associated purely with shear strain can be constructed from invariants of the shear strain tensor $\bar{\mathcal{U}}$. The lowest order invariant of $\bar{\mathcal{U}}$ is the trace:

$$\begin{aligned}\mathrm{tr}\,\bar{\mathcal{U}} &= \frac{1}{2}\left[J^{-2/3}\left(\sum_{i=1}^3 \lambda_i^2 - 3\right) - 3\right] \\ &= J^{-2/3}\left(\frac{\varphi^2}{r^2} + \frac{1}{2}\varphi'^2\right) - \frac{3}{2}.\end{aligned} \tag{23}$$

The lowest order shear strain invariant energy density thus has the form $f_s = \mu'\,\mathrm{tr}\,\bar{\mathcal{U}}$ with μ' a constant. Following Shokef and Safran [25], one can extend this expression to include shear hardening by imposing a maximum shear strain $1/\eta$ through

$$\begin{aligned}f_s &= \mu'\,\mathrm{tr}\,\bar{\mathcal{U}}\left(\frac{1}{1 - \eta\,\mathrm{tr}\,\bar{\mathcal{U}}}\right) \\ &\simeq \mu'\,\mathrm{tr}\,\bar{\mathcal{U}}(1 + \eta\,\mathrm{tr}\,\bar{\mathcal{U}} + \eta^2\,(\mathrm{tr}\,\bar{\mathcal{U}})^2 + ...).\end{aligned} \tag{24}$$

The constant μ' can be identified by going to the limit of infinitesimal deformations. Expanding in powers of the strain tensor of linear elasticity theory, $u_{ij} = \frac{1}{2}(\frac{\partial u_i}{\partial x_j} + \frac{\partial u_j}{\partial x_i})$ [Eq. (7)]:

$$\mu'\mathrm{tr}\,\bar{\mathcal{U}} \simeq \mu'\left(u_{ik} - \tfrac{1}{3}\delta_{ik}u_{ll}\right)^2 + O(u^3). \tag{25}$$

In linear elasticity theory, the elastic energy density of an isotropic material has the form [24]

$$f_{\mathrm{LE}} = \frac{\mu}{4}\left(\frac{\partial u_i}{\partial x_j} + \frac{\partial u_j}{\partial x_i} - \frac{2}{3}\delta_{ij}\frac{\partial u_i}{\partial x_j}\right)^2 + \frac{1}{2}\kappa\left(\frac{\partial u_k}{\partial x_k}\right)^2, \tag{26}$$

with μ the shear modulus and κ the compressional modulus. The first term corresponds to the trace of the nonlinear shear strain tensor, so it follows that one can equate μ' with the shear modulus μ of linear elasticity theory.

III. NEO-HOOKEAN ELASTICITY AND CAVITATION

Before discussing cavitation in gels, it is useful to first examine the simpler case of cavitation in materials that obey neo-Hookean elasticity. The elastic energy density of a neo-Hookean materials generalizes the energy density of isotropic materials according to linear elasticity [Eq. (26)] by replacing the linearized strain tensor $\mathcal{U}_{\mathrm{lin}}$ with the full Green-Lagrange strain tensor $\mathcal{U}$. The resulting elastic energy density can be expressed in terms of the invariants I_1 and J as

$$\begin{aligned}f_{\mathrm{NH}} &= \mu\,\frac{1}{2}\left[J^{-2/3}\left(\sum_{i=1}^3 \lambda_i^2\right) - 3\right] + \frac{\kappa}{2}\,\frac{1}{J}\,(1 - J)^2 \\ &= \mu\left[J^{-2/3}\left(\frac{\varphi^2}{r^2} + \frac{1}{2}\varphi'^2\right) - \frac{3}{2}\right] + \frac{\kappa}{2}\,\frac{1}{J}\,(1 - J)^2,\end{aligned} \tag{27}$$

with $J = \frac{\varphi^2}{r^2}\varphi'$ [26]. The first term is the shear strain energy density contribution and the second term the contribution from changes in density. Shear-strain hardening is included by replacing this first term with Eq. (24). The second term can be expressed in the deformed space as $\frac{\kappa}{2}(\rho/\rho_0 - 1)^2$. The Jacobian J has to be included to allow for the transformation of volume elements when going from the deformed to the reference space.

The deformation map $\varphi(r)$ is determined by minimization of the functional

$$F[\varphi] = \gamma\left(4\pi R_0^2\right) - P\left(\frac{4\pi}{3}R_0^3\right) + F_{\mathrm{el}}[\varphi]. \tag{28}$$

Here, P is the pressure inside the cavity and γ represents a surface tension of the cavity, which is treated as an external force per unit area. The last term is the elastic energy:

$$F_{\mathrm{el}}[\varphi] = 4\pi\int_{r_0}^{\infty} dr\; r^2 f_{\mathrm{NH}}. \tag{29}$$

A. Cavitation in incompressible neo-Hookean systems

The simplest case is the incompressible limit in which case the mapping φ is determined by mass conservation. We also can drop, in this case, the compressional term in the elastic energy density. The resulting elastic energy density is

$$f_{\rm NH} = \mu\left(\frac{\varphi^2}{r^2} + \frac{1}{2}\varphi'^2 - \frac{3}{2}\right). \tag{30}$$

The stretch ratio along the radial direction is

$$\lambda(r) \equiv \frac{\varphi}{r} = \frac{1}{r}\left(r^3 + R_0^3 - r_0^3\right)^{1/3}. \tag{31}$$

The stretch ratio of the surface of the cavity is then $\lambda(r_0) = R_0/r_0$, which we will denote by λ_0. Since $\varphi' = 1/\lambda^2$, one can write the elastic energy density as

$$f_{\rm NH}(r) = \mu\left(\lambda(r)^2 + \frac{1}{2\lambda(r)^4} - \frac{3}{2}\right). \tag{32}$$

The elastic energy $F_{\rm el}$ is given by

$$\begin{aligned} F_{\rm el} &= 4\pi\int_{r_0}^{\infty} dr\, r^2 f(r) \\ &= 4\pi\mu\int_{r_0}^{\infty} dr\, r^2\left(\lambda^2 + \frac{1}{2\lambda^4} - \frac{3}{2}\right). \end{aligned} \tag{33}$$

Change the integration variable from r to λ using

$$\lambda(r) = \frac{1}{r}\left(r^3 + R_0^3 - r_0^3\right)^{1/3} \Rightarrow r(\lambda)^3 = \frac{R_0^3 - r_0^3}{\lambda^3 - 1} \tag{34}$$

and

$$d\lambda = \frac{1}{r}\left(\varphi' - \frac{\varphi}{r}\right)dr = -\frac{\lambda - \lambda^{-2}}{r}dr \Rightarrow \frac{dr}{r} = -\frac{\lambda^2}{\lambda^3 - 1}d\lambda. \tag{35}$$

This gives

$$\begin{aligned} F_{\rm el} &= 4\pi\mu\left(R_0^3 - r_0^3\right)\int_1^{\lambda_0} d\lambda\left(\frac{\lambda}{\lambda^3 - 1}\right)^2\left(\lambda^2 + \frac{1}{2\lambda^4} - \frac{3}{2}\right) \\ &= 4\pi\mu r_0^3\left[\frac{5}{6}\lambda_0^3 - \lambda_0^2 + \frac{1}{2\lambda_0} - \frac{1}{3}\right]. \end{aligned} \tag{36}$$

Minimization of the full energy F with respect to λ_0 gives

$$\left(\frac{5}{2} - \frac{P}{\mu}\right)\lambda_0^2 + 2\left(\frac{\gamma}{\mu r_0} - 1\right)\lambda_0 - \frac{1}{2\lambda_0^2} = 0, \tag{37}$$

so

$$P/\mu = \left(\frac{2\gamma}{\mu r_0}\right)\frac{1}{\lambda} + \left(\frac{5}{2} - \frac{2}{\lambda} - \frac{1}{2\lambda^4}\right). \tag{38}$$

where we dropped the subscript of λ_0. The first term of Eq. (38) is the Laplace capillary pressure. In the following, surface tension will be expressed in dimensionless form as $\bar\gamma = \frac{\gamma}{\mu r_0}$ [27]. The second term reproduces the known relation between pressure and radial extension for cavitation in incompressible materials [11]. The physical meaning of Eq. (38) can be illustrated by expanding it to second order in the dimensionless radial displacement $\epsilon = \lambda - 1 = (R_0/r_0 - 1)$. This gives

$$P/\mu = 2\bar\gamma + (4 - 2\bar\gamma)\epsilon + (-7 + 2\bar\gamma)\epsilon^2 + O(\epsilon^3) \tag{39}$$

The zeroth order term $2\bar\gamma$ is the Laplace capillary pressure of the original cavity. The first-order term $(4 - 2\bar\gamma)\epsilon$ is the result that would have been obtained if one had used linear elasticity and expanded the Laplace Law pressure to first order in ϵ. If one keeps only the zeroth order and first-order terms for a cavity that is not under pressure (so, for $P = 0$), then the radial strain is $\epsilon = -2\bar\gamma/(4 - 2\bar\gamma)$. This is a *negative* quantity, which is reasonable since the capillary pressure exerted by surface tension should cause the radius of an unpressurized cavity to shrink. The second-order term $(2\bar\gamma - 7)\epsilon^2$ is the lowest-order nonlinear correction term. It states that, for $\bar\gamma$ less than $7/2$, the actual cavity radius will be larger than the radius obtained from linear elasticity. The effect of finite-strain elasticity is thus to *soften* the material.

This softening is the key to the cavitation effect. It can be illustrated by a toy model for a balloon treated as a thin spherical elastic shell of radius R composed of a two-dimensional lattice of N harmonic springs with equilibrium spacing a_0. The shell is under an interior pressure $P_{\rm shell}$. By minimizing the total energy, it is easy to show that the pressure is related to the radial extension $\lambda = R/R_0$, where $R_0 \sim N^{1/2}a_0$, by

$$P_{\rm shell}(\lambda)/P_0 = \left(\frac{1}{\lambda} - \frac{1}{\lambda^2}\right).$$

Here, P_0 is proportional to the spring constant and inversely proportional to R_0. Expanding $P_{\rm shell}(\lambda)$ again in powers of the radial displacement $\epsilon = (\lambda - 1)$ produces a term proportional to ϵ with a positive coefficient and a term proportional to ϵ^2 with a negative coefficient, just as for Eq. (38). For the shell case, $P_{\rm shell}/P_0$ has, as a function of λ, a maximum at $\lambda = 2$ after which it decreases to zero in the limit of large λ. Thermodynamic stability requires that the derivative of pressure with respect to volume must be positive. Because $P_{\rm shell}$ decreases with λ for $P > 2P_0$, that section of the curve corresponds to an energy maximum. It follows that the stable section for $P < 2P_0$ actually is only metastable. The unstable section describes energy maxima that correspond to the transition states that need to be crossed before spontaneous bursting of the elastic shell [28].

Does Eq. (38) describe a scenario similar to the bursting of a pressurized elastic shell? Equation (38) has a finite pressure solution when we set λ to infinity, namely, $P_\infty = \frac{5}{2}\mu$, independent of surface tension. This the known critical cavitation pressure of the rubber elasticity literature. Figure 2 shows that the radial extension $(R_0 - r_0)/r_0$ diverges continuously as the pressure P approaches P_∞, provided $\bar\gamma$ is less than one.

There are no other solutions for $\bar\gamma$ less than one. These plots are, in fact, fully stable solutions, so cavitation is physically quite different from the bursting of a pressurized shell.

If $\bar\gamma$ is larger than one, then the cavity radius does not diverge at $P = P_\infty$. For $P > P_\infty$, there are again two solution branches, similar to the case of pressurized shells. One of these—the bottom one in Fig. 2—is stable since the radius increases with pressure while the top branch is unstable as the radius decreases with increasing pressure. This absence of a divergence at P_∞ seems mathematically puzzling since $\lambda = \infty$ *is* a solution of Eq. (38) at P_∞. However, if $\bar\gamma > 1$, then Eq. (38) acquires *additional* solutions at $P = P_\infty$. One of these, $\lambda = \frac{1}{4(\bar\gamma - 1)^{1/3}}$, is real and it is this solution that

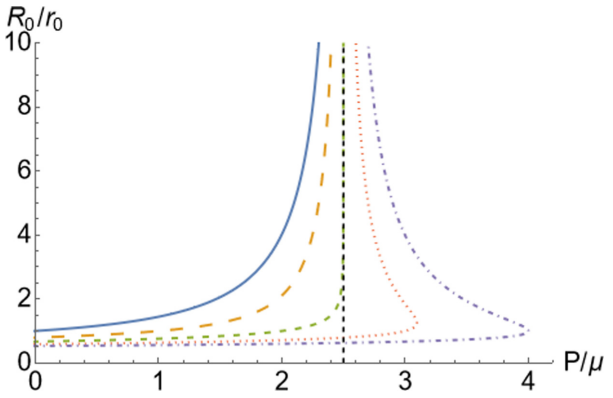

FIG. 2. Dimensionless cavity pressure P/μ versus radial extension ratio for an incompressible system for different values of the dimensionless surface tension $\bar{\gamma} = \gamma/\mu r_0$. The surface tension values are $\bar{\gamma} = 0$ (solid, blue); $\bar{\gamma} = 0.5$ (dashed, yellow); $\bar{\gamma} = 1$ (dashed, green); $\bar{\gamma} = 1.5$ (dotted, red); and $\bar{\gamma} = 2$ (dash-dotted, purple). The dashed black line shows the critical pressure $P_\infty = \frac{5}{2}\mu$.

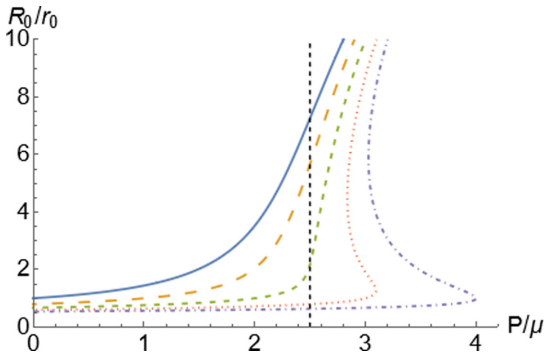

FIG. 3. Dimensionless cavity pressure P/μ versus radial extension ratio for an incompressible system for various values of the dimensionless surface tension $\bar{\gamma} = \gamma/\mu r_0$ and strain-hardening parameter $\eta = 0.01$. The dimensionless surface tensions are $\bar{\gamma} = 0$ (solid, blue); $\bar{\gamma} = 0.5$ (dashed, yellow); $\bar{\gamma} = 1$ (dashed, green); $\bar{\gamma} = 1.5$ (dotted, red); and $\bar{\gamma} = 2$ (dash-dotted, purple). The dashed black line shows the critical pressure $P_\infty = \frac{5}{2}\mu$.

corresponds to the lower branch for $P > P_\infty$. As for the elastic shell, the lower branch is metastable with the upper branch corresponding to a transition-state energy maximum that separates the metastable state from the actual minimum energy state with infinite radius. The metastable solution survives under increasing pressure up to a maximum radius $r_0/(\bar{\gamma} - 1)^{1/3}$ when the two branches fuse. Droplet growth for $\bar{\gamma} > 1$ sequence is consistent with the nucleation-and-growth scenario of conventional phase separation. There is thus a well-defined transition between cavitation for $\bar{\gamma} < 1$ and nucleation for $\bar{\gamma} > 1$.

Shear strain hardening is included by extending the neo-Hookean energy density through the use of Eq. (24) for shear strain energy density. There are two limiting cases. If $\eta^{1/2}\lambda$ is small compared to one, then one can use the perturbation series in powers of the inverse maximum shear strain η. To second order in η, one obtains [29]

$$P(\lambda)/\mu \simeq \left(\frac{2\gamma}{\mu r_0}\right)\frac{1}{\lambda} + \left(\frac{5}{2} - \frac{2}{\lambda} - \frac{1}{2\lambda^4}\right) + \eta\left[4\lambda - \frac{177}{20} + \frac{6}{\lambda} - \frac{2}{\lambda^2} + \frac{3}{2\lambda^4} - \frac{2}{5\lambda^5} - \frac{1}{4\lambda^8}\right] + O(\eta^2\lambda^3). \tag{40}$$

The zeroth order term in η reproduces Eq. (38) for $\eta = 0$. The first-order term (second line) has a term that diverges linearly in the limit of large λ. This will dominate over the zeroth order term, which is finite in the limit of large λ. The second-order term (not shown explicitly) diverges even faster, as λ^3. Higher powers in λ appear as one includes higher order terms in the perturbation expansion in η. Next, in the limit that $\lambda\eta^{1/2}$ approaches one, the integral in the elastic energy is determined by the singularity at $\lambda\eta^{1/2} = 1$ with the result that the pressure diverges in this limit as

$$P(\lambda)/\mu \simeq \frac{\eta^{1/2}}{2(1 - \lambda\eta^{1/2})}. \tag{41}$$

Figure 3 shows the relation between cavity radius and pressure for a strain hardening parameter $\eta = 0.01$ up to and including the second-order term in the expansion in η. The figure is restricted to λ values for which the third-order term in η can be neglected. The divergence of the radius at $P/\mu = \frac{5}{2}\mu$ has disappeared. For increasing γ, the elastic energy again develops a maximum. Beyond a threshold pressure, the radius again increases discontinuously but the radius now does not diverge. Instead, it saturates at a finite value. There is thus still a transition to nucleation-type behavior for larger $\bar{\gamma}$ and for dimensionless pressures larger than 5/2 but droplets no longer expand without limit. For large values of the pressure, $\lambda = R_0/r_0$ increases less rapidly and eventually levels off as it approaches the maximum strain $1/\eta$, according to Eq. (41).

B. Cavitation of neo-Hookean Ccompressible systems

For compressible systems, the deformation map $\varphi(r)$ is not known ahead of time. We used the following variational form:

$$\varphi(r) = r + (R_0 - r_0)\left(\frac{1 + b + c}{\left(\frac{r}{r_0}\right)^2 + b\frac{r}{r_0} + c}\right), \tag{42}$$

with b and c variational parameters. To see why this form is reasonable, note first that it obeys the required condition $\varphi(r_0) = R_0$. Next, the elastic strain must go to zero in the limit of large r, so the theory of linearized elasticity should become valid in this limit. It is a textbook problem to show that, within linear elasticity, the displacement field $u(r)$ surrounding a pressurized spherical cavity embedded in an infinite volume has the form $u_{\rm lin}(r) = A(r_0/r)^2$ with amplitude $A = (R_0 - r_0)$ [24]. For the present nonlinear case, the asymptotic amplitude A is expected to have a different, renormalized value. For $r \gg r_0$, the displacement field $u(r) \equiv \varphi(r) - r$ of the variational deformation map goes to zero as $1/r^2$ with amplitude $A = (R_0 - r_0)(1 + b + c)$. If $b + c > 0$, then the amplitude of the asymptotic strain field exceeds that of linear elasticity theory while for $b + c < 0$ it is reduced. Next, mass conservation requires that, as the cavity expands, material is pushed radially outward, which could produce an excess density at the

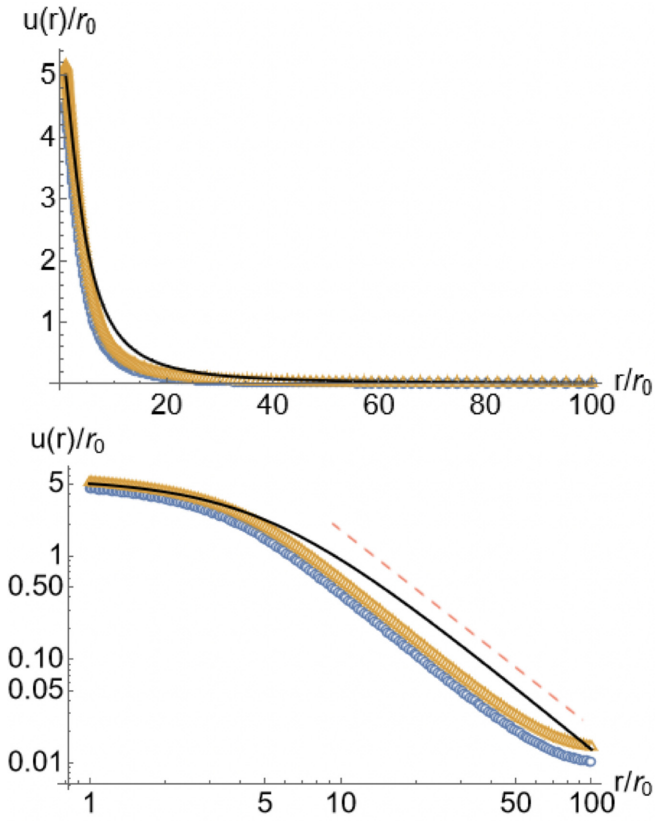

FIG. 4. Top: (black line) $u(r)/r_0 = (\varphi(r) - r)/r_0$ for a cavity radial extension of 6 as obtained by the variational method. The result is compared with $u(r)/r_0$ obtained by the finite element method (FEM) for cavity radial extensions of 5.52 (blue), respectively, 6.16 (gold), as carried out on a spherical sample with outer radius of $100r_0$. Bottom: Same data but plotted on a log-log scale. The red dashed line has the slope of a $1/r^2$ power law.

cavity surface (snowplow effect). On the other hand, lateral stretching could produce a density deficit (balloon effect). The density at $r = r_0$ is given by

$$\frac{\rho(r_0)}{\rho_0} = \frac{(r_0/R_0)^2}{\varphi'(r_0)} = \frac{(r_0/R_0)^2}{\left[1 - (R_0 - r_0)\frac{2+b}{1+b+c}\right]}. \tag{43}$$

If $2 + b$ is positive, then the surface density is increased with respect to ρ_0 while it is decreased if $2 + b$ is negative. The variational ansatz thus allows the density at the cavity surface and the asymptotic amplitude far from the surface to act as separate parameters in the variation.

The variation parameters b and c were obtained by numerical minimization of the elastic energy $F[\varphi]$. Figure 4 shows the results.

The dimensionless displacement $u(r)/r_0 = (\varphi(r) - r)/r_0$ is shown as a function of r/r_0 on a linear-linear scale (top, black line) and on a log-log scale (bottom, black line) for the case of $\lambda = 6$. These variational results are compared with the outcomes of a numerical solution of the equation for mechanical equilibrium [see Eq. (A5)] using the finite-element method (FEM). This was done for cavity radial extensions of 5.52 (blue) and 6.16 (gold) that straddled $\lambda = 6$. The linear-linear plot shows that the agreement is reasonable for r/r_0 less than

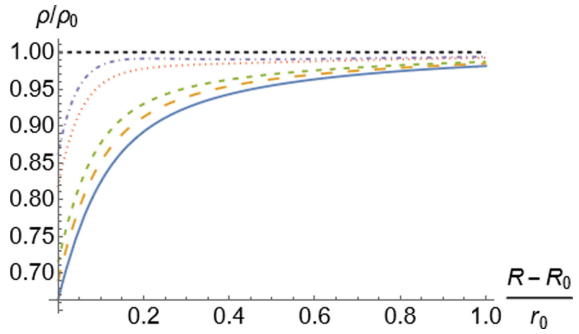

FIG. 5. Relative density ρ/ρ_0 versus distance from cavity surface for the neo-Hookean model for various values of the ratio κ/μ: $\kappa/\mu = 0.1$ (blue, solid); $\kappa/\mu = 0.5$ (yellow, dashed); $\kappa/\mu = 1$ (green, dashed); $\kappa/\mu = 5$ (red, dotted); and $\kappa/\mu = 10$ (purple, dash-dotted). The final cavity radius was twice that of the initial radius.

about five. The log-log plot shows that for $5 \lesssim r/r_0 \lesssim 50$ the FEM radial extension is also consistent with a $1/r^2$ power law. However, the FEM results have a negative ofset with respect to the variational results, which means that the values of the asymptotic amplitudes A do not agree. Finally, the FEM result has an upturn for the largest values of r.

Starting with the last issue, the FEM analysis necessarily had to be done for a finite system. Stress-free boundary conditions were imposed at an outer radius R_2, which was set to $100r_0$. To obey this outer boundary condition, the large r displacement field must—according to linear elasticity—have the form $u(r) = ar + b/r^2$, where $a = b/R_2^3$ [24]. The linear term ar becomes comparable with the b/r^2 term when r is of the order of the outer radius R_2, which explains the upturn in the deformation map for $r \simeq R_2$. The reason for the negative offset of the FEM has to be different because introducing a stress-free boundary condition should produce a larger, not a smaller radial extension. It is discussed in Appendix B that the FEM software package appears to be less reliable for large values of κ/μ.

Using the variational deformation map, one can construct other physical quantities. The density profile, obtained through the relation $\rho_r = \frac{r^2}{\varphi(r)^2\varphi'(r)}$, is shown in Fig. 5.

In all cases, there is a *density deficit*, indicating that the balloon effect overcomes the snowplow effect. For increasing values of κ/μ, the density deficit decreases and the density profiles approach the limit $\rho_r = 1$ of incompressible materials (the FEM method produces a density excess at the cavity surface, see Appendix B).

Next, the relation between pressure P and radial extension is obtained by inserting the variational deformation map into the elastic free-energy density of Eq. (27). After integration over the volume to obtain $F_{\rm el}[\phi]$, the total free energy $F[\phi]$ is minimized with respect to R_0. The result is shown in Fig. 6. Cavitation is encountered for all values of κ/μ. The cavitation critical pressure is significantly reduced for lower values of κ/μ. Compressibility effects thus enhance cavitation. In contrast, for low pressures, the radial extension of the cavity is practically independent of the κ/μ ratio.

Figure 7 shows the effect of varying the surface tension for $\kappa/\mu = 1$. The plots are quite similar to the case of

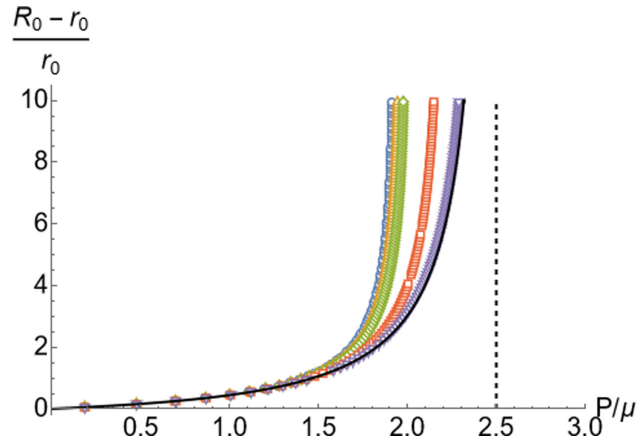

FIG. 6. Radial extension ratio versus dimensionless cavity pressure P/μ for the neo-Hookean model for various values of the ratio of bulk and shear moduli: $\kappa/\mu = 0.1$ (blue, solid); $\kappa/\mu = 0.5$ (yellow, dashed); $\kappa/\mu = 1$ (green, dashed); $\kappa/\mu = 5$ (red, dotted); and $\kappa/\mu = 10$ (purple, inverted triangles). The solid black curve is the incompressible solution, while the dashed black line shows the critical pressure $P_\infty = \frac{5}{2}\mu$.

incompressible materials, apart from the fact that the critical pressure is reduced. Just as for incompressible materials, surface tension can transform cavitation into nucleation and growth above a threshold value of the dimensionless surface tension $\bar{\gamma}$, except that this threshold value now is less than one.

Figure 8 shows what happens if one includes shear hardening for $\eta = 0.1$ and no surface tension. The plots of Fig. 8 show cavitation behavior in the presence of strain hardening in the case that the κ/μ ratio is less than about one. Recall that for incompressible systems, cavitation was suppressed even for a shear hardening parameter that was ten times smaller than the current value of $\eta = 0.1$. Once again, one sees that compressibility promotes cavitation.

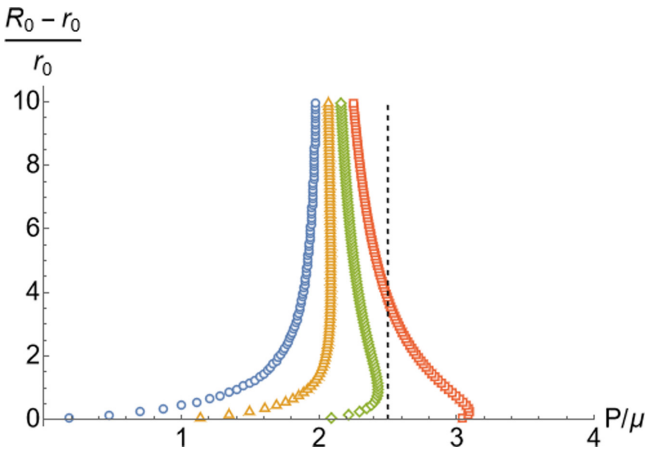

FIG. 7. Radial extension ratio versus dimensionless cavity pressure P/μ for the neo-Hookean model for $\kappa/\mu = 1$ and various values of the dimensionless surface tension $\bar{\gamma} = \gamma/\mu r_0$: $\bar{\gamma} = 0$ (blue, circles); $\bar{\gamma} = 0.5$ (yellow, triangles); $\bar{\gamma} = 1$ (green, diamonds); and $\bar{\gamma} = 1.5$ (red, squares). There is no shear hardening.

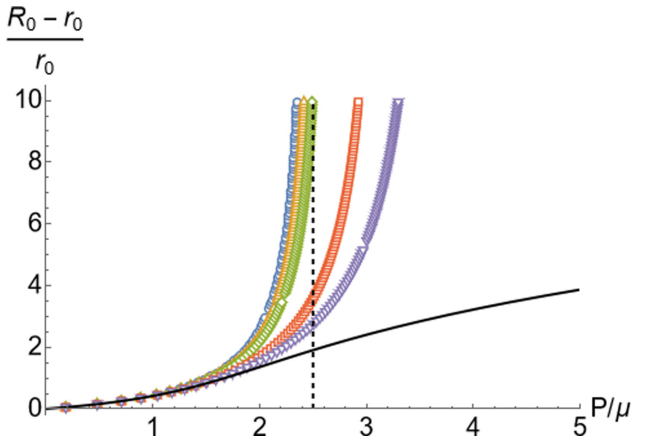

FIG. 8. Radial extension ratio versus dimensionless cavity pressure P/μ for the neo-Hookean model for shear hardening parameter $\eta = 0.1$, no surface tension, and various values of κ/μ: $\kappa/\mu = 0.1$ (blue, circles); $\kappa/\mu = 0.5$ (yellow, triangles); $\kappa/\mu = 1$ (green, diamonds); $\kappa/\mu = 5$ (red, squares); and $\kappa/\mu = 10$ (purple, inverted triangles). The solid black curve represents the incompressible solution, while the dashed black line shows the critical pressure $P_\infty = \frac{5}{2}\mu$.

IV. CAVITATION IN POLYMER GELS WITH TWO-COMPONENT SOLVENTS

With this experience, we now can turn to the actual case of interest, namely, cavitation in polymer gels. From the viewpoint of finite-strain elasticity theory, there is an important new ingredient. A cross-linked polymer gel placed in a one-component solvent can swell or shrink by absorbing or releasing solvent. On the one hand, in good solvent the free energy associated with volume interactions between the monomers and the solvent molecules decreases under swelling. On the other hand, swelling stretches the polymer chains, which reduces entropic configurational entropy. In the state of *swelling equilibrium*, the swelling pressure is balanced by the elastic stress of the stretched polymers [16,30]. The state of swelling equilibrium is not stress-free, so it cannot serve as the reference frame. In the theory of gel elasticity, the stress-free reference state is the *dry*, solvent-free gel with no solvent and hence no stretching of the polymer chains [31] and no surface energy.

Now, let the solvent be a two-component binary liquid where the majority component is a good solvent for the monomers of the gel while the minority component is a poor solvent. In the absence of the gel, the thermodynamic work of formation of a minority phase droplet in a homogeneous supersaturated binary solution equals $W = -N\Delta\mu + F_{\rm ex}$. Here, $N = V/v_0$ is the number of molecules in the droplet, V is the volume of the droplet, v_0 is the molecular volume of the minority phase molecules, and N the number of minority molecules in the droplet. Next, $\Delta\mu$ is the difference between the chemical potential of minority phase molecules in the homogeneous mixture and those inside the drop. Finally, $F_{\rm ex}$ is the increase of the free energy of the surrounding environment due to the presence of the drop. In classical nucleation theory (CNT), only the interfacial energy of the droplet is included in $F_{\rm ex}$, so $F_{\rm ex} = \gamma A$ where γ is the interfacial energy

per unit area and A the surface area of the drop. The radius R^* of the droplet in a stationary state in which the droplet neither grows nor shrinks is determined by the condition that the virtual work δW associated with an infinitesimal change of the droplet radius is equal to zero [32]. The positive work by the chemical potential is given by $\delta N \Delta\mu = \delta V(\Delta\mu/v_0)$, where $\Pi = \Delta\mu/v_0$ can be interpreted as an osmotic pressure that drives droplet swelling. The total work δW associated with an infinitesimal change δR of the radius R of the droplet is then

$$\delta W = \gamma \delta A - \Pi \delta V, \tag{44}$$

where $\delta A = 8\pi R \delta R$ and where $\delta V = 4\pi R^2 \delta R$. The radius of the stationary droplet is then $R^* = (2\gamma/\Pi)$, which is known as the critical droplet size in CNT. A stationary point with $\delta W = 0$ represents a thermodynamically stable state only if the derivative of osmotic pressure Π with respect to the cavity volume is positive. The state $\delta W = 0$ is unstable, so smaller droplets shrink and disappear while larger drops grow without limit.

Next, assume that the droplet nucleates in a solvent-filled cavity inside a gel that is originally in a state of swelling equilibrium. Let the initial radius be r_0. Once the radius of the growing droplet exceeds that of the cavity, the work of elastic deformation of the gel by the growing droplet must be included as an additional excess free-energy term $F_{\rm ex}$. The condition $\delta W = 0$ for a stationary corresponds to the stationary state of the variational free energy expression $F[\phi]$ [see Eq. (29)], provided P is interpreted as an osmotic pressure and γ as an interfacial free energy (below, we will use P for the osmotic pressure of the drop).

A. Flory-Huggins theory and cavitation

To compute the elastic deformation energy $F[\phi]$ of the gel, we will use the Flory-Huggins (FH) mean-field theory of gels in which the polymer chains are treated as ideal Gaussian chains composed of N_x identical segments [31]. It has been established that the physical properties of gels composed of *flexible* polymers are well described by FH theory, which also can be extended to include liquid-liquid phase separation [7]. In FH theory, the free energy density is the sum of the entropic elasticity free energy of the Gaussian chains and the mixing free energy of the monomers [16,30]:

$$f_{\rm FH} = \frac{1}{2} C_1(\phi)\left(\sum_{i=1}^{3} \lambda_i^2 - 3\right) + \frac{k_b T}{w}[(1-\phi)\ln(1-\phi) + \chi\phi(1-\phi)], \tag{45}$$

where we followed the notation of Refs. [16,31]. Here, ϕ is the volume fraction of monomers where $\phi = 1$ is the state of the dry, solvent-free gel. Next, $C_1(\phi)$ equals $\frac{k_B T \phi}{w N_x}$, where w is the volume per Kuhn segment of the polymer chains. The quantities λ_i are, as before, the three principal stretch ratios such that in the dry state the stretching parameters are equal to one. For a uniformly swollen gel, the stretch parameters are equal to each other and to $\phi^{-1/3}$ because of mass conservation. Finally, χ is the Flory χ parameter. For good solvents, the Flory parameter is less than $1/2$. Note that this is the free-energy density in the deformed space. Note also that, unlike the neo-Hookean elastic energy, the FH free energy density is not the sum of separate shear and compression or swelling terms since the first term of $f_{\rm FH}$ describes simultaneously the energy cost of stretching the polymers both under shear strain and under isotropic swelling.

The state of swelling equilibrium is found by minimizing f/ϕ with respect to ϕ. The appearance of the factor $1/\phi$ is understood here by noting that the volume element dV in the physical space of the swollen gel transforms to the the volume element $dv = \phi dV$ in the dry gel so f/ϕ is the free energy density in the coordinate system of the dry gel. Minimizing f/ϕ with respect to ϕ gives, for $N_x \gg 1$, the result is that $\phi_{\rm eq} \simeq [(1/2 - \chi)N_x]^{-3/5}$. This same result is obtained if one sets the osmotic pressure $\Pi(\phi) = \phi^2 \frac{d(f/\phi)}{d\phi}$ of the gel to zero, where

$$\Pi(\phi) = -\frac{k_B T}{w}\left[(\chi\phi + 1)\phi + \log(1-\phi) + \frac{\phi^{1/3}}{N_x}\right]. \tag{46}$$

If the deformation away from the state of swelling equilibrium is infinitesimal, then the free-energy density associated with the deformation has the same form as the elastic energy density of uniform materials that obey linear elasticity [see Eq. (26)]. The shear modulus is given by

$$\mu = \frac{k_B T}{w N_x}\phi^{1/3} \tag{47}$$

and the osmotic modulus $\kappa = \phi \frac{d\Pi}{d\phi}$ by

$$\kappa = \frac{k_B T}{w}\left(\left(\frac{1}{1-\phi} - 2\chi\right)\phi^2 - \frac{\phi^{1/3}}{3N_x}\right) \tag{48}$$

(see Ref. [31]). For an FH gel, shear and bulk moduli are thus replaced as control parameters by the number of polymer segments N_x per link and the Flory χ parameter, the latter a measure of the solubility of the polymers in terms of the majority component of liquid.

B. Cavitation without strain hardening or surface tension

The density profile in an FH gel surrounding a minority phase droplet under osmotic pressure is found in the same way as for neo-Hookean materials. Results for the case of no interfacial energy and no strain hardening are shown in Fig. 9. This density profile has a maximum near the cavity surface. For FH gels, the snowplow effect apparently overcomes lateral stretching, just the opposite of what we found for neo-Hookean materials. The density profile is quite dependent on the Flory χ parameter. The excess density at the surface increases as the solubility of the polymers for the mixed phase decreases (i.e., for more negative values of χ), which agrees with physical intuition.

Figure 10 shows the dependence of radial extension on cavity pressure. The radial extension plots for different values of N_x and χ are surprisingly similar and close to that of incompressible materials (black line). Differences become visible only for dimensionless pressures close to the critical $5/2$ ratio for incompressible materials.

A plot of the ratio of bulk and shear moduli of the FH model as a function of χ is shown in Fig. 11. For N_x

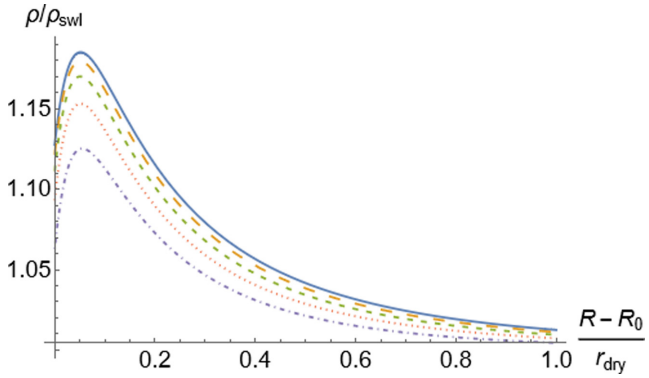

FIG. 9. Relative density $\rho/\rho_{\rm swl}$ versus distance from cavity surface for the Flory-Huggins model, with final cavity radius twice that at swelling equilibrium, cross-link separation $N_x = 10$, and various values of the Flory χ parameter. The values of χ are $\chi = -0.4$ (solid, blue); $\chi = -0.2$ (dashed, yellow); $\chi = 0$ (dashed, green); $\chi = 0.2$ (dotted, red); and $\chi = 0.4$ (dash-dotted, purple).

large compared to one, the ratio of bulk and shear moduli approaches 5/3 for χ less than 1/2, independent of either χ or N_x. Since the ratio of the shear and bulk moduli of an FH gel near swelling equilibrium is of the order of one, one would have expected a significant reduction of the critical cavitation pressure as compared to that of incompressible materials, based on the earlier results for the neo-Hookean model, but this is not the case. Another surprise is the persistent lack of dependence of the radial extension on the Flory χ parameter and N_x outside the regime where linear elasticity holds. Recall that the density profile did not show this universality.

Figure 12 shows the effect of surface tension on the radial extension versus pressure plot and compares it with incompressible materials. The effect of surface tension on cavitation

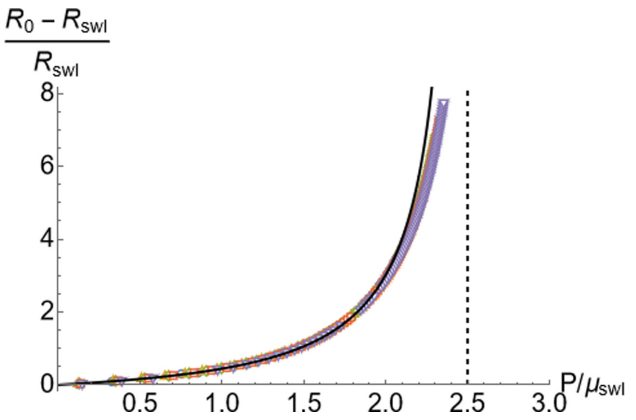

FIG. 10. Radial extension ratio with respect to the equilibrium state versus dimensionless cavity pressure $P/\mu_{\rm swl}$ for the Flory-Huggins model with $\mu_{\rm swl}$ the shear modulus at swelling equilibrium. The cross-link separation is $N_x = 10$ and there is neither surface tension nor shear hardening. The values of the Flory χ parameter are $\chi = -0.4$ (blue, circles); $\chi = -0.2$ (yellow, triangles); $\chi = 0$ (green, diamonds); $\chi = 0.2$ (red, squares); and $\chi = 0.4$ (purple, inverted triangles). The black line shows the relation between radial extension and pressure for an incompressible material.

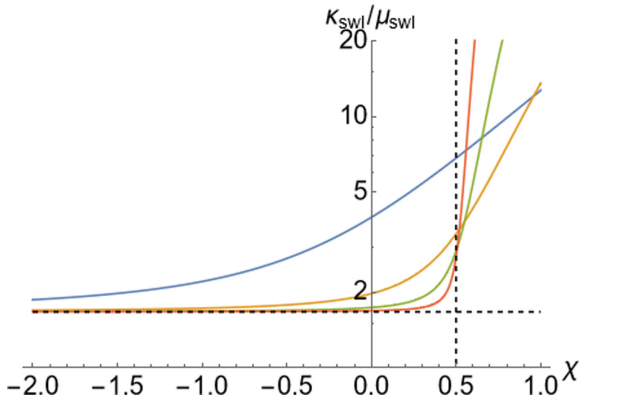

FIG. 11. Dependence of the ratio of shear and bulk moduli of the FH model at swelling equilibrium on the Flory χ parameter for different values of N_x: $N_x = 1$ (blue); $N_x = 10$ (yellow); $N_x = 100$ (green); and $N_x = 1000$ (red).

in FH gels is practically the same as the effect of surface tension on cavitation for incompressible systems.

Next, we include strain hardening. Because in the FH free-energy density, shear strain, and expansion or compression strain both contribute to the first term, we cannot include strain hardening only in the shear strain. We included strain hardening by replacing the first term of $f_{\rm FH}$ by

$$C_1(\phi)\mathrm{tr}\mathcal{U}(1 + \eta\,\mathrm{tr}\mathcal{U} + \eta^2\,(\mathrm{tr}\,x\mathcal{U})^2 + ...), \qquad (49)$$

where $\mathrm{tr}\mathcal{U} = \frac{1}{2}(\sum_{i=1}^{3}\lambda_i^2 - 3)$. Figure 13 shows the effect of this term on plots of the radial extension as a function of pressure. For a strain-hardening parameter $\eta = 0.01$, there is no cavitation, just a somewhat higher rate of radial expansion for higher pressures. Strain hardening suppresses cavitation in FH gels even more effectively than in incompressible systems with the same shear modulus. Next, the radial expansion plots

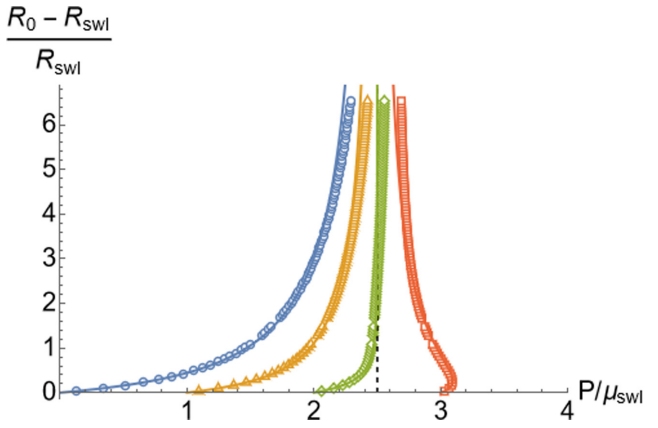

FIG. 12. Radial extension ratio versus dimensionless cavity pressure $P/\mu_{\rm swl}$ for the FH model, with cross-link separation $N_x = 10$, Flory χ parameter $\chi = -0.2$, no shear hardening, and various values of dimensionless surface tension $\bar{\gamma} = \gamma/\mu_{\rm swl}r_{\rm swl}$. The values of $\bar{\gamma}$ are $\bar{\gamma} = 0$ (blue, circles); $\bar{\gamma} = 0.5$ (yellow, triangles), $\bar{\gamma} = 1$ (green, diamonds); and $\bar{\gamma} = 1.5$ (red, squares). The black dashed line shows the critical pressure for the incompressible solution, $P_\infty = \frac{5}{2}\mu_{\rm swl}$. The solid lines show the corresponding radial extension curves of an incompressible material according to Eq. (38).

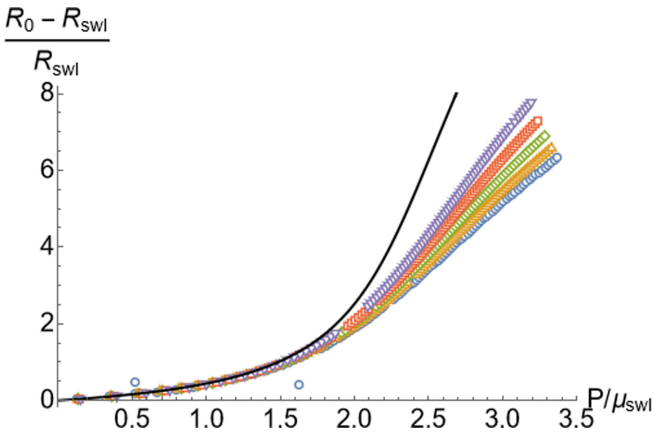

FIG. 13. Radial extension ratio versus dimensionless cavity pressure P/μ_{swl} for FH gels with μ_{swl} the shear modulus at swelling equilibrium, cross-link separation $N_x = 10$, no surface tension, shear hardening parameter $\eta = 0.01$, and various values of the Flory χ parameter: χ are $\chi = -0.4$ (blue, circles), $\chi = -0.2$ (yellow, triangles); $\chi = 0$ (green, diamonds); $\chi = 0.2$ (red, squares); and $\chi = 0.4$ (purple, inverted triangles). The solid black curve shows the radial extension or pressure plot of an incompressible material for the same amount of strain hardening and the same shear modulus [see Eq. (40)].

are now significantly dependent on the Flory χ parameter for higher pressures: The suppression of cavitation becomes more pronounced as the solubility of the polymers for the mixed solvent is reduced. Similarly, if the cross-link separation N_x is increased then the cavitation is suppressed more effectively. This plot must be compared with Fig. 8 for neo-Hookean materials. There, compressibility significantly enhanced cavitation for an η value that was ten times higher than for the present case. Strain hardening suppresses cavitation very effectively for FH gels.

V. CONCLUSION

We applied finite-strain elasticity theory to cavitation in compressible FH gels to explore the effects of strain hardening and droplet surface or interfacial tension on cavitation. The results for FH gels were compared with those for neo-Hookean materials with comparable elastic moduli. In this Conclusion, we briefly review these results and then discuss parameter ranges for different cases and implications for experiment.

The effect of surface tension on cavitation is described by the dimensionless parameter $\bar{\gamma} = \frac{\gamma}{\mu r_0}$. If $\bar{\gamma}$ is less than a number close to one, then the effects of surface tension on cavitation are secondary but if $\bar{\gamma}$ is greater than that number then cavitation is replaced by activated droplet nucleation and growth. What are reasonable values for $\bar{\gamma}$? Biomolecular condensates in aqueous environments have interfacial energies in the range of 10^{-4} mN/m to 10^{0} mN/m [33]. If the cavity radius r_0 for the dry gel is estimated to be of the order of the size of a monomer of a synthetic flexible polymer (of the order of one nm) and μ is taken to be of the order of the G' modulus of hydrogels (about 10^3 Pa), then $\bar{\gamma}$ falls in the range of 0.1 to 10^3. However, the estimate of the cavity radius of a dry gel is uncertain and it probably will be larger for less flexible polymers, so this parameter may have to be used as a fitting parameter. Despite this uncertainty, the estimate indicates that both cases are possible. It may be possible to distinguish the two cases experimentally on the basis of the statistically broad range of waiting times associated with activated growth kinetics for $\bar{\gamma}$ greater than one versus the case of continuous cavity swelling for $\bar{\gamma}$ less than one.

This transition between discontinuous, activated bursting for $\bar{\gamma} > 1$ and continuous cavitation if $\bar{\gamma} < 1$ has an interesting similarity with the tricritical point encountered in the theory of phase transitions when a line of continuous phase transitions transforms into a line of first-order phase transitions [34]. It would be interesting to investigate experimentally the regime $\bar{\gamma} \simeq 1$ and $P/\mu \simeq 5/2$ in more detail to see if there is a tricritical point for phase separation in polymer gels near the transition point between cavitation and nucleation.

Our second important result is that compressibility significantly reduces the critical cavitation pressure of neo-Hookean materials, provided the compressional modulus is comparable to (or less than) the shear modulus. For FH gels on the other hand, the critical cavitation pressure is practically the same as that of incompressible materials. Because the shear and compressional moduli of an FH gel are comparable at swelling equilibrium, this was surprising. Actually, the elastic properties of FH gels were also in other respects more similar to incompressible materials than to a compressible materials with similar elastic moduli. We encountered this in the case of surface tension, strain hardening, and density profile. The fact that the deformation map of an incompressible material is a reasonable approximation for that of a gel with a pressurized cavity is convenient. It allows one to easily include effects such as strain hardening and surface tension [see Eq. (40)]. The observation that FH gels behave in some respects as incompressible materials was actually made before in an experimental study of the response of hydrogels to externally applied osmotic pressure [35]. The proposed explanation there was that this effect is due to the *prestress* in the state of swelling equilibrium. The hydrogel did not respond significantly to external pressures that were small compared to the internal stress. In general, prestressed materials (like prestressed concrete) are much less responsive to external stress than materials that are stress-free prior to the application of the external stress. While the response of biogels to shear stress has been extensively studied, there is little literature on measurements of prestress in biogels, though *in vitro* observations on thermal fluctuations of biogel filaments would suggest that prestress is small. *Active* gels, such as *in vitro* actin-myosin solutions in the presence of Adenosine triphosphate (ATP), certainly do have significant internal stresses and it would be very interesting to know how such systems respond to osmotic pressure and whether they show cavitation when placed in a two-component solvent.

Our key result is that cavitation in FH gels is *very sensitive* to strain hardening. We found that cavitation is suppressed for strain hardening parameters η as small as 0.01. Typical synthetic polymer gels composed of highly flexible polymers with a low level of cross-linking densities show no observable strain hardening [18]. Next, synthetic biomimetic gels

show various levels strain hardening depending on the material but, for example, synthetic gels composed of triblock copolymers [20] have effective η values in the range of one. Similarly, biomimetic DA/PDA hydrogels have η values in the range of ten [18]. Next, for a sequence of actin, collagen, fibrin, vimentin, and neurofilaments biopolymer networks, measured η values decrease from about ten (actin) to about 0.1 (neurofilaments) [17]. Shear hardening in biogels strongly depends on the cross-linking density. For collagen gels, the η value increased from about 10^1 to about 10^3 under increasing cross-linking density [36]. All of these η values are well above 0.01. This would mean that none of these systems ought to show cavitation according to our results. It could be countered that biogels are composed of semi-flexible polymer, whose osmotic properties may differ from FH gels. The experimental literature on the osmotic properties of biomimetic gels composed of semiflexible polymers is quite small, but the osmotic properties of gels composed of cross-linked DNA appear to obey FH [37]. This question will have to be addressed experimentally.

If our claim is confirmed, then this would seem to indicate that cavitation is not relevant for biogels. In actuality, the biopolymer networks of the cell are *transiently* cross-linked. The shear modulus and strain-hardening properties of viscoelastic materials such as these are dependent on the timescale on which they are measured: they become increasingly more fluidlike on longer timescales. A slow-motion, viscoelastic version of cavitation thus seems quite possible and we hope to investigate this question in the future.

We finish by noting that cavitationlike phenomena may involve mechanisms that we did not discuss. Reference [38] discusses the effects of finite segregation strength. If the difference $\Delta\gamma$ between the interfacial energies per unit area of the polymer material with minority and majority solvent components is sufficiently small, then it is expected that, instead of cavitation, growing droplets may permeate the polymer network. The authors argue that cavitation requires the so-called permeoelastic number given by $p = 2\phi\Delta\gamma/(r\mu)$ to be larger than a number of the order of one (r is here the polymer radius and μ the shear modulus). They estimate that for synthetic biogels, like silicone gels in an oil-water mixture, p is large compared to one while p is small compared to one for the cytoplasm. For the interior of the nucleus, p may or may not be large compared to one. It should be noted though that even if a droplet permeates the polymer matrix, then this *still* induces strains in the polymer matrix. These strains could well be large compared to one for small ϕ. It would be interesting to investigate if one could have a hybrid form of permeation and cavitation. Finally, the elastic stress at the surface of the cavity may exceed the fracture stress of the polymer network, producing cavitationlike effects.

True cavitation is, however, of fundamental interest as a phenomenon that is present in non-linear, finite-strain elasticity theory but that is absent in conventional linear elasticity. Synthetic biogels now seem to provide us with the opportunity for precision experimental studies of cavitation that allow us to test finite-strain elasticity theory at small length scales.

Note added. In the course of preparation of this article, one of the co-authors, Alex Levine, passed away.

ACKNOWLEDGMENTS

A.J.L. acknowledged partial support from NSF-DMR-1709785. R.B. would like to thank the NSF-DMR for continued support under CMMT Grant No. 1836404. We would like to thank Sam Safran and Yair Shokef for a useful discussion.

APPENDIX A: CAUCHY AND FIRST PIOLA-KIRCHHOFF STRESS TENSORS

The definition of a stress tensor starts from the surface element $d\vec{S} = dS\,\hat{N}$ in the deformed space with normal unit vector $\hat{N}$. If a force (or traction) $\vec{T}$ is acting on this surface element, then the Cauchy stress tensor σ at the location $\vec{X}$ of this element is defined such that

$$T^i = \sigma^i_j dS^j. \tag{A1}$$

The Cauchy stress tensor is defined in the deformed space, the physical space in which the force is being applied. When external stresses or pressures are applied to the surface of the material then the Cauchy stress tensor provides a direct approach to implement boundary conditions. However, within the Lagrangian formalism that we use, it is useful to also construct a stress tensor in terms of the coordinates of the undeformed space with $\vec{X} = \varphi(\vec{x})$ the deformation map.

Let $\vec{B}$ represent a body force per unit volume, and $\vec{t} = \sigma\hat{N}$ represent a contact force per unit area acting on the surface of the body. Applying Newton's second law to a body in mechanical equilibrium—in the deformed space—gives

$$\int_{\mathcal{B}} dV\; B^i + \int_{\partial\mathcal{B}} dS\; \sigma^i_j N^j = 0. \tag{A2}$$

Using the divergence theorem, one can write this in local form as

$$\frac{D\sigma^{ij}}{DX^j} + B^i = 0. \tag{A3}$$

Changing variables in the integral equation to those of the undeformed space gives

$$\int_{\mathcal{B}_0} dv\; JB^i + \int_{\partial\mathcal{B}_0} ds\; J(A^{-1})^\alpha_{\ j} n_\alpha \sigma^{ij} = 0. \tag{A4}$$

Define the *first Piola-Kirchoff stress tensor* $S^{i\alpha} \equiv J(A^{-1})^\alpha_{\ j}\sigma^{ij}$. Using the divergence theorem, this can be expressed as a local equation for mechanical equilibrium:

$$\frac{DS^{i\alpha}}{Dx^\alpha} + JB^i = 0. \tag{A5}$$

The deformation map φ is obtained by solving this equation.

Summarizing the definitions:

Deformation map: $\vec{X} = \varphi(\vec{x})$.

Deformation gradient matrix: $A^i_{\ \alpha} = \frac{\partial\varphi^i}{\partial x^\alpha}$.

Green-Lagrange strain tensor: $\mathcal{U}^\alpha_\beta \equiv \frac{1}{2}(A^{i\alpha}A_{i\beta} - \delta^\alpha_\beta)$

Jacobian: $J = \frac{\rho_0}{\rho} = \det A$.

Nonlinear shear strain tensor:

$\bar{\mathcal{U}}^\alpha_\beta = \frac{1}{2}(J^{-2/3}A^{i\alpha}A_{i\beta} - \delta^\alpha_\beta)$

$= J^{-2/3}\mathcal{U}^\alpha_\beta + \frac{1}{2}(J^{-2/3} - 1)\delta^\alpha_\beta$

Cauchy stress tensor: σ^i_j.

Piola-Kirchoff stress tensor: $S^{i\alpha} = J(A^{-1})^\alpha_{\ j}\sigma^{ij}$.

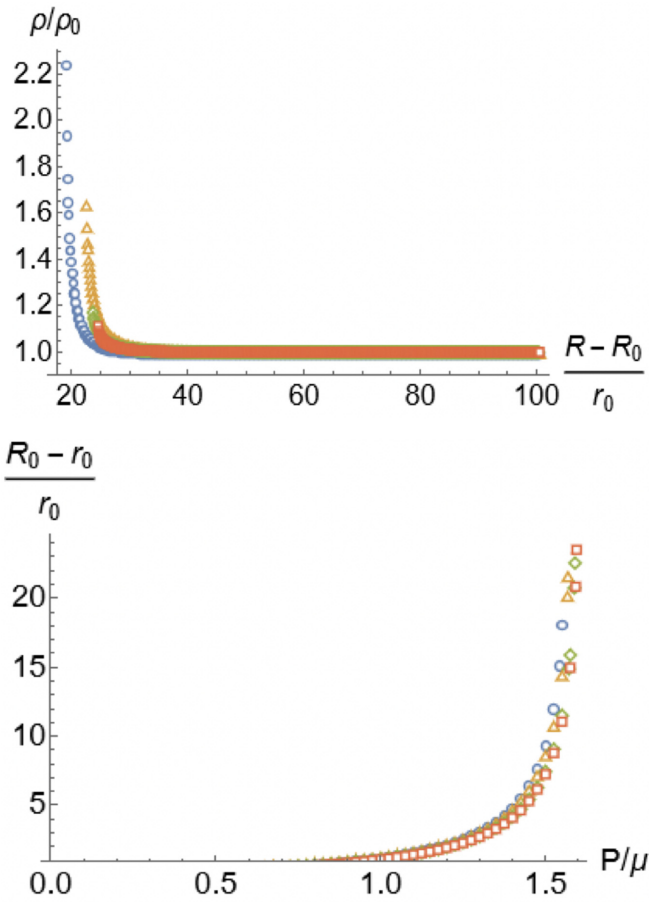

FIG. 14. Top: Radial density profiles obtained from the finite-element method (FEM) for different values of the ratio κ/μ between bulk and shear moduli. Bottom: Cavity extension versus dimensionless cavity pressure P/μ using the FEM, for the same values of κ/μ. The values of κ/μ are 0.5 (blue circles), 1 (yellow triangles), 5 (green diamonds), and 10 (red squares).

APPENDIX B: FINITE ELEMENT METHOD AND THE VARIATIONAL ANSATZ

We used the FEBIO STUDIO [39] software package to perform a finite element analysis for a sphere with a concentric spherical cavity made up of a compressible neo-Hookean material. The simulations were force controlled, i.e., the pressure acting on the surface of the cavity was an input and displacements of the nodes of the finite element mesh were the output. We used 20-node quadratic hexahedral elements. Taking advantage of the spherical symmetry of the problem, we modeled only one-eighth of the sphere with appropriate symmetry boundary conditions. We chose the outer radius of the sphere to be 10^2 times the radius of the cavity. We checked for convergence by comparing the critical pressure for a mesh with 3552 elements and a mesh with 24 057 elements. The resulting deformation map was shown in the main text and compared with the map obtained by the variational method. The density profile and radial extension or pressure profiles obtained by the FEM are shown in Fig. 14. According to the top figure, there is a density excess instead of the density deficit that was obtained by the variational method. According to the bottom figure, there is qualitative agreement between the radial expansion or pressure plots of the FEM and the variational methods. However, the critical cavitation pressure produced by the FEM is significantly smaller than the one predicted by the variational method and appears to be only weakly dependent on κ/μ. In particular, the FEM critical cavitation pressure does not approach the known critical cavitation pressure $P/\mu = 2.5$ of incompressible systems for large values of κ/μ as it should.

The density at the surface of the cavity is determined by the slope $\varphi'(r_0)$ of the deformation map through $\frac{\rho(r_0)}{\rho_0} = \frac{1}{\lambda_0^2\varphi'(r_0)}$. A density excess will occur at the cavity surface if $0 < \varphi'(r_0) < \frac{1}{\lambda_0^2}$ while a density deficit occurs when $\varphi'(r_0) > \frac{1}{\lambda_0^2}$. For $\lambda_0 = 6$, the variational method gives $\varphi'(r_0) \approx 0.1763$, which exceeds $1/\lambda_0^2$, corresponding to a density deficit. The FEM analysis gives $\lambda_0 = 5.52$ and $\varphi'(r_0) \approx 0.0187$, which is less than $1/\lambda_0^2$, and for $\lambda_0 = 6.16$, $\varphi'(r_0) \approx 0.0119$, which is also less than $1/\lambda_0^2$. Both correspond to a surface density excess. So, even though the deformation maps of the variational and FEM methods appear to be similar in the region of smaller r, there is a substantial difference between the slopes of the deformation maps at the cavity surface. This difference produces the difference in signs of the change in density at the cavity surface. The origin of the discrepancy is not clear but because the FEM does not reproduce for large κ/μ the exact result for incompressible systems, we believe that the variational method is more reliable in this case.

[1] C. P. Brangwynne, J. Cell Biol. **203**, 875 (2013).
[2] A. A. Hyman, C. A. Weber, and F. Jülicher, Annu. Rev. Cell Dev. Biol. **30**, 39 (2014).
[3] J. A. Riback, L. Zhu, M. C. Ferrolino, M. Tolbert, D. M. Mitrea, D. W. Sanders, M.-T. Wei, R. W. Kriwacki, and C. P. Brangwynne, Nature (London) **581**, 209 (2020).
[4] D. M. Mitrea, B. Chandra, M. C. Ferrolino, E. B. Gibbs, M. Tolbert, M. R. White, and R. W. Kriwacki, J. Mol. Biol. **430**, 4773 (2018).
[5] M. Hondele, S. Heinrich, P. De Los Rios, and K. Weis, Emerging Top. Life Sci. **4**, 343 (2020).
[6] S. Boeynaems, S. Alberti, N. L. Fawzi, T. Mittag, M. Polymenidou, F. Rousseau, J. Schymkowitz, J. Shorter, B. Wolozin, L. Van Den Bosch *et al.*, Trends Cell Biol. **28**, 420 (2018).
[7] X. Wei, J. Zhou, Y. Wang, and F. Meng, Phys. Rev. Lett. **125**, 268001 (2020).
[8] P. W. Voorhees, J. Stat. Phys. **38**, 231 (1985).
[9] Y. Zhang, D. S. W. Lee, Y. Meir, C. P. Brangwynne, and N. S. Wingreen, Phys. Rev. Lett. **126**, 258102 (2021).
[10] R. W. Style, T. Sai, N. Fanelli, M. Ijavi, K. Smith-Mannschott, Q. Xu, L. A. Wilen, and E. R. Dufresne, Phys. Rev. X **8**, 011028 (2018).

[11] A. Gent and C. Wang, J. Mater. Sci. **26**, 3392 (1991).
[12] C. W. Barney, C. E. Dougan, K. R. McLeod, A. Kazemi-Moridani, Y. Zheng, Z. Ye, S. Tiwari, I. Sacligil, R. A. Riggleman, S. Cai *et al.*, Proc. Natl. Acad. Sci. **117**, 9157 (2020).
[13] K. A. Rosowski, E. Vidal-Henriquez, D. Zwicker, R. W. Style, and E. R. Dufresne, Soft Matter **16**, 5892 (2020).
[14] A. E. Green and W. Zerna, *Theoretical Elasticity* (Dover, New York, 1992).
[15] P.-G. De Gennes and P.-G. Gennes, *Scaling Concepts in Polymer Physics* (Cornell University Press, Ithaka, New York, 1979).
[16] M. Doi, *Introduction to Polymer Physics* (Oxford University Press, Oxford, 1996).
[17] C. Storm, J. J. Pastore, F. C. MacKintosh, T. C. Lubensky, and P. A. Janmey, Nature (London) **435**, 191 (2005).
[18] M. F.-C. Romera, *Biomimetic Strain-Stiffening Hydrogels* (Technische Universiteit Eindhoven, Eindhoven, 2018).
[19] J. Gu, Y. Guo, Y. Li, J. Wang, W. Wang, Y. Cao, and B. Xue, Int. J. Mol. Sci. **23**, 3032 (2022).
[20] K. A. Erk, K. J. Henderson, and K. R. Shull, Biomacromolecules **11**, 1358 (2010).
[21] M. Jaspers, M. Dennison, M. F. Mabesoone, F. C. MacKintosh, A. E. Rowan, and P. H. Kouwer, Nat. Commun. **5**, 5808 (2014).
[22] R. W. Ogden, *Non-Linear Elastic Deformations* (Dover, New York, 1997).
[23] J. E. Marsden and T. J. R. Hughes, *Mathematical Foundations of Elasticity* (Dover, New York, 1994).
[24] L. D. Landau and E. M. Lifshitz, *Theory of Elasticity*, 3rd ed., Course of Theoretical Physics Vol. 7 (Elsevier, Amsterdam, 1986).
[25] Y. Shokef and S. A. Safran, Phys. Rev. Lett. **108**, 178103 (2012).
[26] The $1/J$ factor in the second term is normally dropped in the engineering literature but that is not appropriate for highly compressible materials.
[27] This definition of the dimensionless surface tension differs from the elastocapillary number of Ref. [7].
[28] For a serious application of finite strain elasticity theory to the swelling of balloons, see Ref. [40].
[29] See Supplemental Material at http://link.aps.org/supplemental/10.1103/PhysRevE.107.024418 for the steps of the calculation.
[30] M. Rubinstein and R. H. Colby, *Polymer Physics* (Oxford University Press New York, New York, 2003), Vol. 23.
[31] M. Doi, J. Phys. Soc. Jpn. **78**, 052001 (2009).
[32] D. Kashchiev, J. Chem. Phys. **76**, 5098 (1982).
[33] H. Wang, F. M. Kelley, D. Milovanovic, B. S. Schuster, and Z. Shi, Biophysical Reports **1**, 100011 (2021).
[34] P. M. Chaikin and T. C. Lubensky, *Principles of Condensed Matter Physics* (Cambridge University Press, Cambridge, 1995).
[35] A. Bhattacharyya, C. O'Bryan, Y. Ni, C. D. Morley, C. R. Taylor, and T. E. Angelini, Biotribology **22**, 100125 (2020).
[36] D. Vader, A. Kabla, D. Weitz, and L. Mahadevan, PloS one **4**, e5902 (2009).
[37] F. Horkay and P. J. Basser, Biomacromolecules **5**, 232 (2004).
[38] P. Ronceray, S. Mao, A. Košmrlj, and M. P. Haataja, Europhys. Lett. **137**, 67001 (2022).
[39] S. A. Maas, B. J. Ellis, G. A. Ateshian, and J. A. Weiss, J. Biomech. Eng. **134**, 011005 (2012).
[40] I. Müller and P. Strehlow, *Rubber and Rubber Balloons: Paradigms of Thermodynamics* (Springer Science & Business Media, Berlin, Heidelberg, 2004), Vol. 637.